LASER INTERFEROMETER GRAVITATIONAL WAVE OBSERVATORY
-LIGO-

CALIFORNIA INSTITUTE OF TECHNOLOGY
MASSACHUSETTS INSTITUTE OF TECHNOLOGY

Technical Note	**LIGO-T-980069-00-D**	**July 23, 1998**

Lock Acquisition Final Design

Brent Ware, Lisa Sievers
ware@ligo.caltech.edu, lisa@willyluna.jpl.nasa.gov

This is an internal working note
of the LIGO Project.

California Institute of Technology
LIGO Project - MS 51-33
Pasadena CA 91125
Phone (626) 395-2966
Fax (626) 304-9834
E-mail: info@ligo.caltech.edu

Massachusetts Institute of Technology
LIGO Project - MS 20B-145
Cambridge, MA 01239
Phone (617) 253-4824
Fax (617) 253-7014
E-mail: info@ligo.mit.edu

WWW: http://www.ligo.caltech.edu/

file /home/ware/docs/isc/fdr.ps - printed July 23, 1998

1 Lock Acquisition

Lock acquisition is the process by which the six pendulum-mounted masses which comprise a recycled Fabry-Perot interferometer are constrained from their initial condition of swinging about wildly due to ground motion ('wildly', here, means tens of microns), which give a signal only in the brief moments when their random juxtaposition fulfills the resonance conditions of the (varying) laser frequency, and using feedback to stop their motion within that ephemeral resonance condition.

The design criteria by which this is done are constrained by several considerations, not all of which are independent of the others. The feedback control system which is optimal for the low-noise gravitational detection mode operation of the interferometer is not suitable for lock acquisition, so a different set of controllers must be designed.

2 Design Considerations

There are several constraints of the interferometer which unavoidably affect the properties of the lock acquisition controller design. Among these are:

- Parameters – optics, stacks, pendula, etc. – which are optimized for gravity wave detection
- seismically-induced motion
- internal modes of optics
- physical limits on actuator/sensors

Within these constraints, the design of the acquisition mode must meet the requirements of

- Short mean time to lock
- Robustness against seismically-induced motion
- Stability

2.1 Acquisition time

The overriding concern of the lock acquisition system is to acquire lock within a reasonably short time[1]. 'Reasonably short' is of course open to interpretation, but the Mean Time to Lock (MTTL) should be small enough that it does not hinder the operation of the interferometer, which is taken to mean that MTTL is a small fraction of average time the IFO is locked. Paradoxically, this implies the importance of a short MTTL is most important in the initial days of LIGO when the IFO will almost certainly fall out of lock constantly. So lock acquisition must work reliably and robustly from the initial LIGO turn-on.

Though it can be calculated in a general manner from the probability distribution of the velocities of the masses given the observed ground motion, a first-order estimate of lock time can be found by thinking of the length difference between a pair of test masses as a free particle in a gas inside a box of dimension $\lambda/2$ (the distance between fringes). If $x_{\text{fringe}} \ll \lambda/2$, and $x_{\text{fringe}} \ll x_{\text{mean free path}}$, then the probability distribution function of the position of the particle may be taken as uniform. The mean

[1] Unlike the gravitation detection mode, noise is of very little concern to this portion of the design.

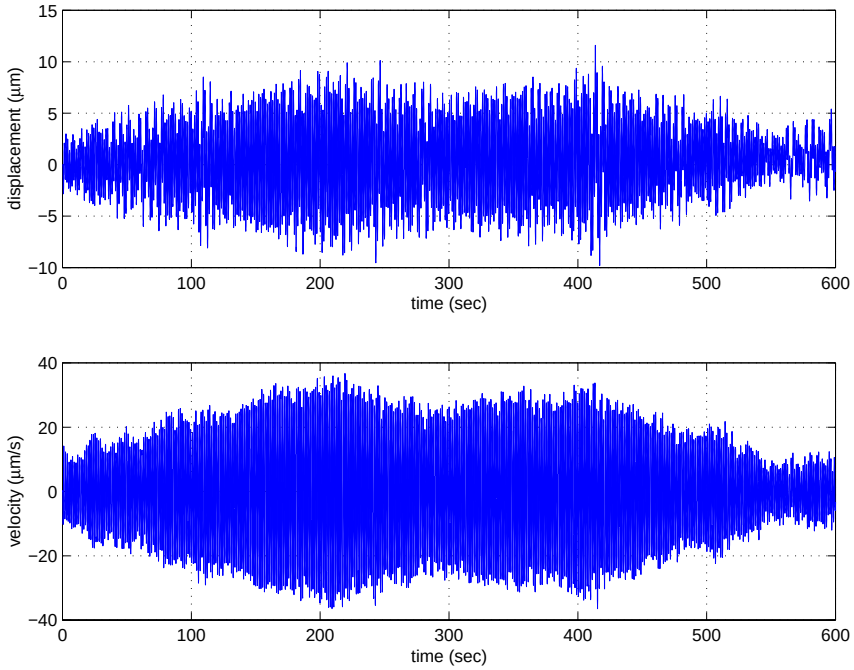

Figure 1: Time series of L_- displacement and velocity at the Livingston site (measured ground motion filtered through a simulated stack and pendulum) [2].

free path of the particle, the distance it moves before it changes direction (Fig. 1), is large enough, on the order of microns, that the probability that the particle will change directions within the fringe is small. The width of the fringe is $\lambda/2\mathcal{F}$, or 2.6 nm. Then

$$\tau_{\rm lock} \sim \frac{\lambda/2}{v_{\rm thr}\, P(v < v_{\rm thr})} \tag{1}$$

where the threshold velocity, $v_{\rm thr}$, is the velocity below which the controllers will always acquire lock.

From measurements of ground motion at Livingston and Hanford [1], the worst case $v_{\rm rms} \sim 5\ \lambda$/s. If $v_{\rm thr} \simeq 1\ \lambda$/s, then $P(v < v_{\rm thr}) \approx 0.15$, which implies a $\tau_{\rm lock}$ on the order of seconds. The relative ground motion of L_- is the driving consideration, as this motion is on the order of 30 μm peak-to-peak. The motion of the $l_\pm$ degrees of freedom is much less, on the order of nm, and so is much less of a concern. The requirement of $v_{\rm thr} \geq 1\ \lambda$/s is then the figure of merit here.

2.2 Acquisition states

Extensive simulation with the SMAC simulator [3] has shown that there is a preferred sequence to lock acquisition [1]:

State 1 Masses swinging wildly about, no resonant buildup.

State 2 Sideband resonant within the recycled Michelson cavity.

State 3 Sideband resonant within the recycled Michelson cavity and the carrier resonant within the in-line arm.

State 4 Sideband resonant within the recycled Michelson cavity and the carrier resonant in both Fabry-Perot arms.

This sequence of events is shown in Fig. 2. This figure also shows two pseudo-lock resonant states, States 2sb and 3sb. Unless controllers are configured to acquire these states, there is no danger of the interferometer locking in either of these pseudo-states; their significance lies in the possibility of disrupting the acquisition sequence as the interferometer passes through these resonant conditions.

2.3 Stability

The high threshold velocity necessary for short MTTL in turn requires high bandwidth in the acquisition controllers. As the velocity increases, the time spent in the fringe decreases, and the bandwidth necessary to actuate on the motion in time to correct it increases. Unfortunately, I have not yet derived an explicit relationship between threshold velocity, bandwidth, and gain, nor had the opportunity to explore this phase space systematically with SMAC, though experience indicates that increasing both the gain and bandwidth results in higher threshold velocities.

The relationship between the velocity of masses in a F-P cavity and the zero crossings of the fringe has been found, both theoretically and experimentally, to be [4]:

$$\tau_{12} \simeq \left(\sqrt{2}-1\right)\left[\left(\frac{2L_0}{c}\right)\left(\frac{\lambda}{v}\right)\right]^{1/2} \begin{cases} L_0 = 4 \text{ km} \\ \lambda = 1.06\ \mu\text{m} \end{cases} \tag{2}$$

where τ_{12} is the time between the first and second minima of the fringe.

From SMAC simulations, this relationship is found to be

$$\tau_{12} = \frac{2.1}{\sqrt{v}} \text{ ms} \qquad \text{(velocity in } \mu\text{m/s)}, \tag{3}$$

within 5% of the predicted value.

2.4 Ground noise

The requirements on the open loop gain of the system are determined by the ground motion of the system, and the ability to acquire and maintain lock in the presence of this noise.

The worst-case L_- ground motion recorded has a peak-to-peak amplitude of 20 μm (Fig. 1) at 0.2 Hz and 2 Hzafter filtering through stack and pendulum. The width of a fringe is $\lambda/2\mathcal{F} = 1.064 \times 10^{-6}/2(208) = 2.6$ nm. So the open loop gain needed to reduce the ground motion to the width of a fringe is $x_{\text{gnd}}/x_{\text{fringe}} = 2 \times 10^{-5}/2.6 \times 10^{-9} \sim 8 \times 10^3$, or 80 dB. For stable operation, the motion needs to be reduced to some small fraction of the fringe width. 10% was chosen arbitrarily, corresponding to a required gain of 100 dB at microseismic frequencies.

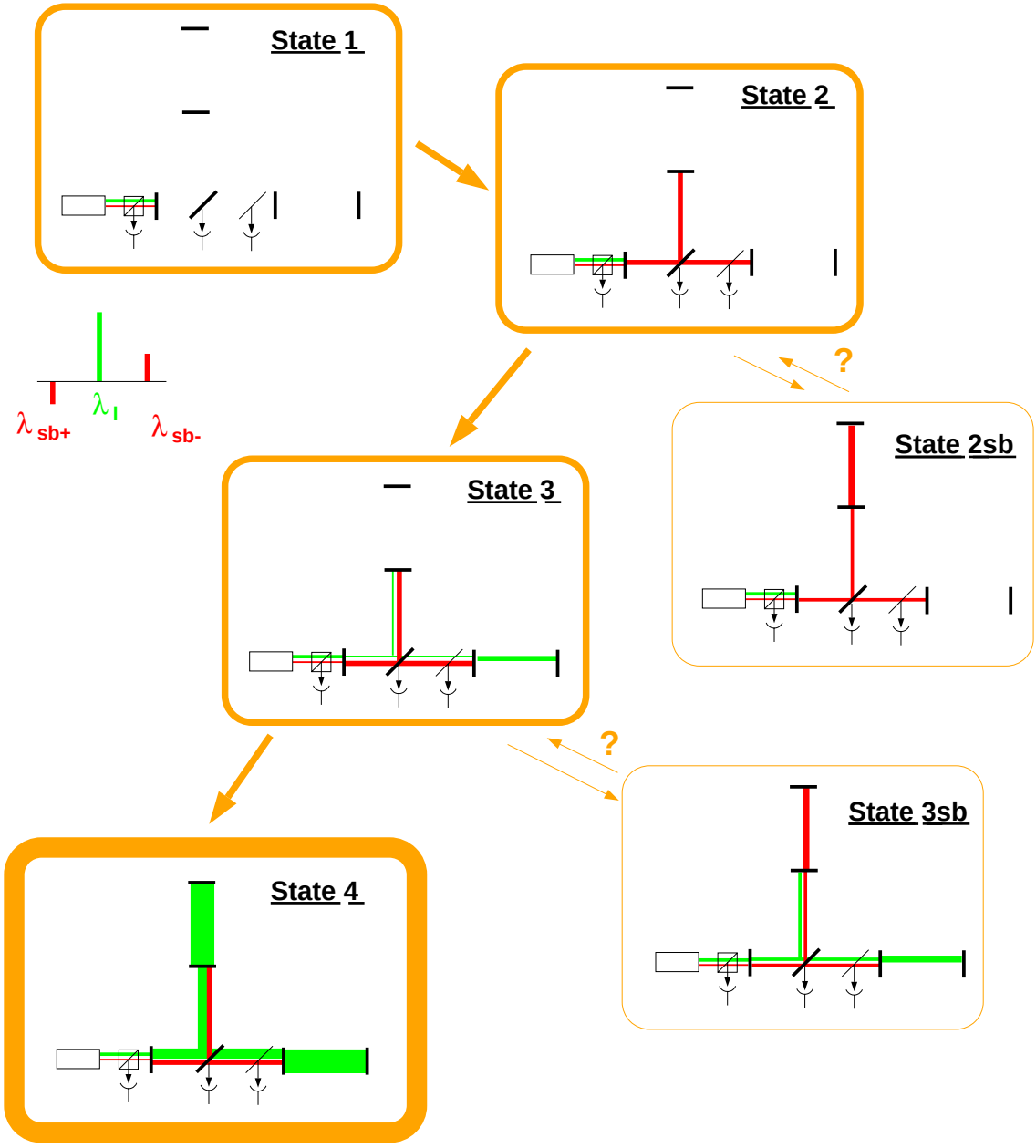

Figure 2: Acquisition locking sequence, definition of acquisition states.

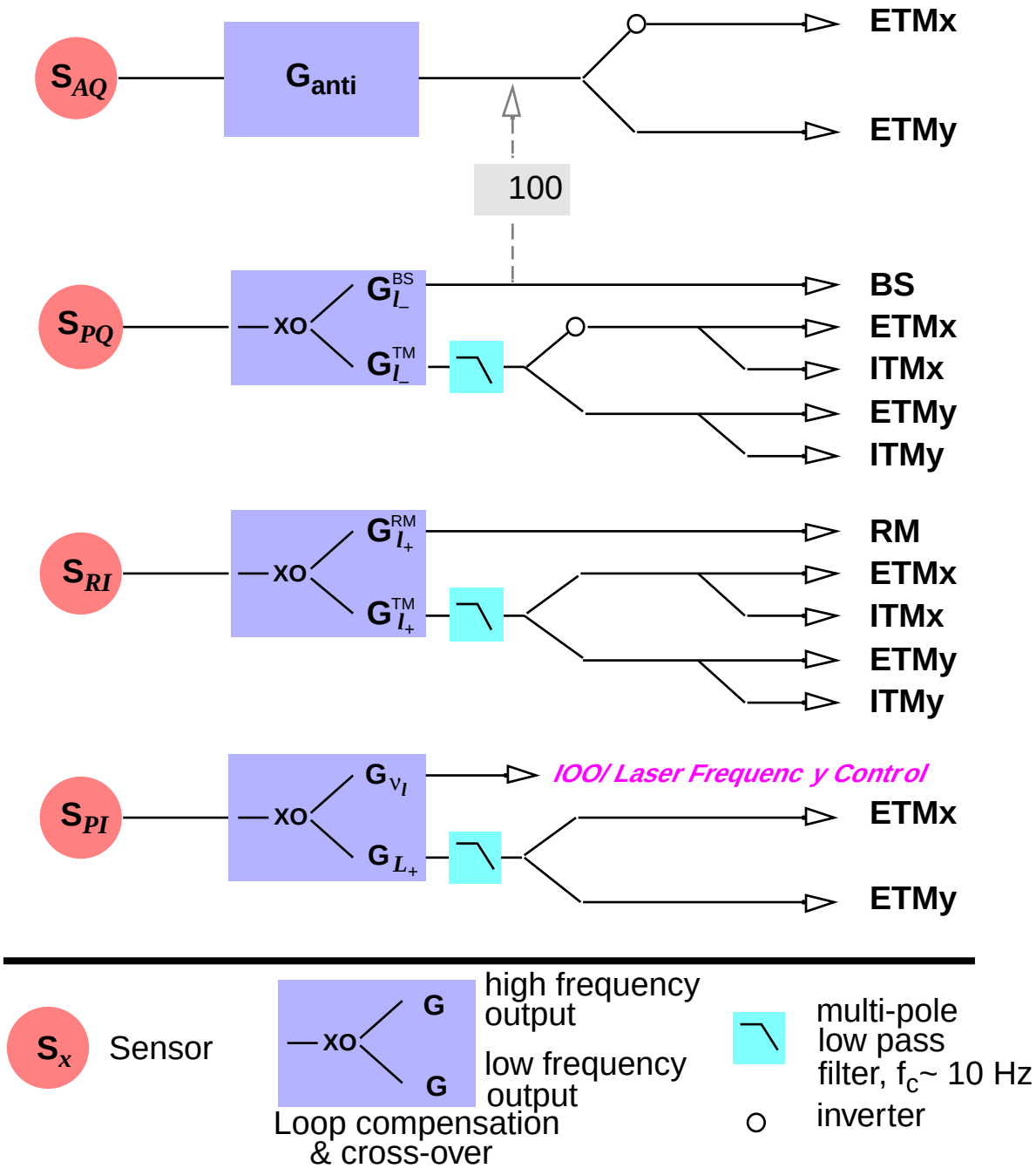

Figure 3: Sensor/actuator configuration – S_{PI} and S_{RI} are reversed from the detection mode configuration because the amplitude of the fields on the pickoff is down by 30 dB in State 3, when l_+ is needed but L_+ is not.

2.5 Actuator limits

In the following section, the limits on the ranges of the actuators which are actually used are derived. In developing the lock acquisition controllers, these limitations were implemented in the SMAC simulation, so all results are valid with these limitations.

2.5.1 OSEMs

The OSEMs[2] have a force capability of 20 mN/A/coil for each of the four coils [5]. In acquisition mode, the maximum current available is 300 mA. The total force then is $(4)(20 \times 10^{-3})(300 \times 10^{-3}) = 24$ mN per test mass (60×10^{-6} N/V), and $x_{max} = \mathrm{F}_{max}/(m\omega_0^2) = 100$ μm per test mass (twice that per test mass pair corresponding to a length degree of freedom). This gives a gain of 100 μm/400 V = 250 nm/V.

2.5.2 PSL frequency

The frequency of the PSL can be varied by ± 5 MHz [6], so

$$\frac{\mathrm{FSR}}{\delta\nu} = \frac{\lambda/2}{\delta L},$$

where the FSR is 37.4 kHz, giving a laser frequency control of $\delta L(\delta\nu_{max}) = 133.7\lambda$, or approximately 133 fringes. The voltage-controlled oscillator which drives the PSL frequency control has a bandwidth of 100 kHz.

2.6 COC internal resonances

The high frequency response of the controllers is determined by the internal resonances of the test mass. These modes are very high Q, and so must not be excited during acquisition, both because they can destroy the stability of the system, and because, once excited, take a very long time to ring down. The most crucial of these, because of its frequency (very close to the Nyquist frequency) and strength, is the first drumhead mode at 9.4764 kHz, which has a Q of 1.3×10^6 [7]. The time constant of this mode is on the order of a minute, and the time it takes to ring this oscillation up to unity gain

$$t\big|_{0\ \mathrm{dB}} = -\tau_0\ \ln\left[1 - \frac{1}{A_r Q}\right] \tag{4}$$

where A_r is the attenuation at that frequency. Since $\ln\left[1 - \frac{1}{A_r Q}\right] \sim \frac{1}{A_r Q}$ for $A_r \ll Q$, it is easy to see that only when the attenuation is equal to or greater than the Q of the resonance is the system safe from instability. This implies that the open loop gain of the system must be attenuated by at least the Q of the resonance, -122 dB, at the first internal test mass resonance.

2.7 Guided lock

Due to the high threshold velocities achieved, and the low MTTL this implies, guided lock acquisition is not necessary at this time. Nonetheless, the system will be designed with the appropriate hooks so this can be added later.

[2]There is a 1/40 Hz pole-zero pair in the suspension controllers used for detection mode which is switched out for lock acquisition.

2.8 Plant modelling

In order to design real controllers, the IFO plant must be modelled adequately. The frequency response of the sensors to the length DOFs can be found analytically, and from SMAC and Twiddle simulations. The analytical equations and their derivations can be found in [8] and [9]. SMAC was modified to display full Bode plot information, both amplitude and phase. The results of these were compared to Twiddle and to the theoretical calculations of the plant response, and show reasonable agreement (some absolute gain and phase shifts have yet to be resolved).

For purposes of lock acquisition design, the MIMO IFO (Eq. 5) can be treated as diagonal[3], and the controller MIMO system appropriately diagonalized (Eq. 6).

$$\begin{bmatrix} S_{PI} \\ S_{RI} \\ S_{AQ} \\ S_{PQ} \end{bmatrix} = \begin{bmatrix} p_{21} & p_{22} & p_{23} & p_{24} & p_{26} \\ p_{11} & p_{12} & p_{13} & p_{14} & p_{16} \\ p_{31} & p_{32} & p_{33} & p_{34} & p_{36} \\ p_{41} & p_{42} & p_{43} & p_{44} & p_{46} \end{bmatrix} \begin{bmatrix} \phi \\ l_+ \\ L_- \\ l_- \\ L_+ \end{bmatrix} \tag{5}$$

$$\begin{bmatrix} \phi \\ l_+ \\ L_- \\ l_- \\ L_+ \end{bmatrix} = \begin{bmatrix} c_{11} & 0 & 0 & 0 \\ 0 & c_{22} & 0 & 0 \\ 0 & 0 & c_{33} & 0 \\ 0 & 0 & 0 & c_{44} \\ c_{66} & 0 & 0 & 0 \end{bmatrix} \begin{bmatrix} S_{PI} \\ S_{RI} \\ S_{AQ} \\ S_{PQ} \end{bmatrix} \tag{6}$$

3 Differential Modes

3.1 Plant model

For the differential degrees of freedom, and using the LIGO parameters, the full IFO equations reduce to:

$$S_{AQ} \simeq -S\ 40\frac{1}{s+2\pi\,91}\Big[\boldsymbol{\delta L_-} + \epsilon\ \boldsymbol{\delta l_-}\Big] \tag{7}$$

$$S_{RQ} \simeq S\ 2\Big[\epsilon\ \boldsymbol{\delta L_-} + \boldsymbol{\delta l_-}\Big] \tag{8}$$

$$S_{PQ} \simeq S\ 250\Big[\epsilon\ \boldsymbol{\delta L_-} - \boldsymbol{\delta l_-}\Big] \tag{9}$$

where $\epsilon = \pi/2\mathcal{F} \simeq 1/132$ and S is an overall power parameter. If the resonances at the FSR and its harmonics are included (which they must when designing the high bandwidth acquisition controllers), these equations agree with the results found using SMAC and Twiddle.

These are the results for the steady-State 4 plant. The plant transfer functions of the $l_\pm$ DOFs are unchanged between State 2 and 3. In acquisition mode, $l_\pm$ gain is reduced by a factor of 30 from State 4 because of the decreased power buildup in the recycling cavity (300 W vs. 10 W). This 30 dB gain difference is switched during the transition to State 3. There are of course no $L_\pm$ DOFs in either State 2 or 3.

[3]The swap of rows 1 and 2, and the absence of column 5 in Eq. 5 are historical artifacts of the design process.

3.2 Controllers

Now that the plant model is known, and the simulation matches theoretical prediction, this information can be used to design stable controllers. The rules for designing a controller which will acquire lock are, unfortunately, not as well defined as the rules for ensuring stability. The basic requirements are:

- The threshold velocities be as high as necessary to acquire lock in a short time, implying a relatively high bandwidth,
- High gain to acquire and hold lock in the presence of ground motion,
- Unconditional stability, and
- Of lesser importance, commonality with the detection mode controllers.

Given these requirements, the following differential mode controllers were arrived at by modification of proven controllers, inspired guess, and limited exploration of gain/bandwidth phase space.

$$\begin{aligned} c_{33}(S_{AQ} \to L_-) &= -112 \text{ dB } \frac{(s - 2\pi\ 0.1)(s - 2\pi\ 50)(s - 2\pi\ 500)(s - 2\pi\ 1 \text{ kHz})}{(s - 2\pi\ 1)(s - 2\pi\ 2 \text{ kHz})(s - 2\pi\ 3 \text{ kHz})} \\ &\times \quad (6 \text{ pole, } 0.1\% \text{ ripple, } 60 \text{ dB stopband, } 8.0 \text{ kHz elliptic}) \\ &\times \quad (8 \text{ pole } 80 \text{ dB elliptic notch } 9.1 \text{ kHz-}10.1 \text{ kHz}) \end{aligned} \tag{10}$$

$$\begin{aligned} c_{44}\ (S_{PQ} \to l_-) &= -\ 21.6\ \frac{(s - 2\pi\ 2)(s - 2\pi\ 30)}{(s - 2\pi\ 10)(s - 2\pi\ 300)} \\ &\times \quad (2 \text{ kHz } 5 \text{ pole Butterworth}) \end{aligned} \tag{11}$$

The open-loop gains of the resulting system for States 3 and 4 are shown in Figs. 5 (L_-) and Figs. 6 and 7 (l_-).

4 Common Modes

4.1 Plant model

For the common modes, the full interferometer equations reduce to

$$S_{RI} \simeq S\,\frac{1}{\epsilon^2}\,\frac{1}{s + 2\pi\,0.77}\Big[10(s + 2\pi\ 2.9)\,\epsilon^2\,\boldsymbol{\delta l}_+ + \boldsymbol{\delta L}_+\Big] \tag{12}$$

$$S_{PI} \simeq S\,10\frac{1}{s + 2\pi\,0.77}\Big[(s - 2\pi\ 0.86)\,\epsilon\,\boldsymbol{\delta l}_+ - 9\,\boldsymbol{\delta L}_+\Big] \tag{13}$$

The l_+ controller is switched in after State 2 is locked, and L_+ after State 4 is locked.

State Transition	Loop	Trigger	Effect
$1 \rightarrow 2$	l_-	$P^{tr}_{s\|\|}$ & $P^{tr}_{s\perp} \geq 0.4\ \mu$W	State 2 acquired, enable l_+ loop
$2 \rightarrow 3$	$l_\pm$	$P^{tr}_{c\|\|}$ | $P^{tr}_{c\perp} > 0.1$ mW	-30 dB gain, $\pm\ l_\pm$ actuator sign
$3 \rightarrow 4$ (acq)	L_-	$P^r_c < 0.02$ & $P^a_c > 0.1$ W	enable L_- loop
4 (acq) $\rightarrow$ 4 (det)	all	$P^{tr}_{c\|\|}$ & $P^{tr}_{c\perp} > 0.1$ W	switch to detection mode

Table 1: Transition through the acquisition states, showing triggers and controller enabling. c – carrier, s – sideband, tr – transmitted, a – asymmetric port, r – reflected port.

4.2 Controllers

$$c_{11}\ (S_{PI} \rightarrow \phi) \quad = \quad -\frac{1}{10}\ \frac{(s - 2\pi\ 500)(s - 2\pi\ 50\ \text{kHz})}{s(s - 2\pi\ 1)(s - 2\pi\ 10\ \text{kHz})} \tag{14}$$

$$c_{22}\ (S_{RI} \rightarrow l_+) \quad = \quad -\ 1080\ \frac{(s - 2\pi\ 1)(s - 2\pi\ 50)}{(s - 2\pi\ 100)(s - 2\pi\ 300)(s - 2\pi\ 3.5\ \text{kHz})} \tag{15}$$

$$c_{66}\ (S_{PI} \rightarrow L_+) \quad = \quad \text{detection mode} \tag{16}$$

The controller for the PSL frequency has the distinction of being local, and thus not subject to the frequency limitations imposed by the Nyquist limit of the digitized loops; thus the 10 and 50 kHz terms.

The open-loop gains of the resulting system for States 3 and 4 are shown in Figs. 8 and 9 (PSL) and Figs. 10 and 11 (l_+).

5 Triggers and switching

The state of the IFO at any moment is determined by the circulating power in the cavities. The power incident on the sensors measures the circulating power and so can be used to determine state transitions and the appropriate switching of controllers for each state (Figs. 12-15).

As the l_- loop comes into lock and the recycled Michelson cavity becomes resonant with the sideband, the resonant sideband power increases to several watts, and a small fraction of this power is transmitted through the as-yet unresonant Fabry-Perot arms to the transmitted light detectors. This increase in sideband power triggers the closure of the l_+ loop. After the Michelson is locked, the PSL loop then locks onto the in-line arm motion and the carrier becomes resonant within the Michelson and the in-line F-P cavity, State 3. This is detected by the carrier power resonant on the transmitted light sensors both reaching 0.1 mW. This condition enables the L_- loop, which brings the perpendicular arm into resonance with the carrier, State 4. In this condition, the resonant carrier power in each cavity reaches its maximum value, 300 W in the Michelson, and 20 kW in each of the arms.

The triggers used by SMAC for lock acquisition are shown in Table 1.

6 Performance and Results

The performance requirements set out in the beginning of this section and in the PDR have been substantially met.

6.1 MTTL

The crucial DOFs determining the MTTL are the differential mode lengths, L_- and l_-. Since the initial achievement of lock acquisition using SMAC, the L_- threshold velocity of the working design has been increased from 0.3 λ/s to 3.0 λ/s. The l_- threshold velocity has been increased from 0.1 λ/s to 0.5 λ/s. For the former, from Eq. 1, this implies a MTTL of one second. For the latter, the RMS excursion is on the order of 12 nm (150 nm peak-peak), with an RMS velocity of 2.4 nm/s (12 nm RMS displacement/(0.2 Hz)$^{-1}$ – RMS displacement over microseismic time constant), so the probability that the relative velocity of the masses in the l_- cavity is less than $v_{\rm thr}$ (2.4 nm/s vs 0.5 μm/s) is unity, and $t_{\rm lock} = \lambda/(2 \times 0.5) = 1$ second.

While these are estimates, they are consistent with SMAC simulations, and even given some error, should be adequate for initial LIGO turn-on.

6.2 Seismic motion suppression

The crucial degree of freedom here is L_-, and the gain necessary to achieve the desired suppression of ground noise has been implemented. This can be seen in Fig. 4.

6.3 Stability

All lock acquisition controllers have sufficient gain and phase margins to be unconditionally stable[4]. The margins for each controller are shown in Table 2.

7 Things To Do

While a set of controllers have been designed which meet the requirements set out, there are a number of issues which might profitably be explored, some more crucial to initial LIGO turn-on than others.

[4]Due to a late modification of the L_- controller, its gain margin has been decreased somewhat (in order to increase the depth of the test mass resonance notch), but with judicious tweaking, this will be rectified.

CONTROLLER		STATE 3						STATE 4					
		Gain (dB)			Phase (deg.)			Gain (dB)			Phase (deg.)		
c_{11}	$S_{PI} \to \phi$	∞	@	–	43	@	372 Hz	∞	@	–	50	@	13.7 kHz
c_{22}	$S_{RI} \to l_+$	16	@	1.11 kHz	36	@	413 Hz	30	@	1.12 kHz	87	@	110 Hz
c_{33} (acq)	$S_{AQ} \to L_-$		@			@		2	@	2.05 kHz	13	@	1.72 kHz
c_{33} (det)	$S_{AQ} \to L_-$		@			@		18	@	1.28 kHz	45	@	272 Hz
c_{44}	$S_{PQ} \to l_-$	36	@	378 Hz	53	@	18 Hz	31	@	379 Hz	53	@	25 Hz
c_{66}	$S_{PI} \to L_+$												

Table 2: Gain and phase margins of controllers

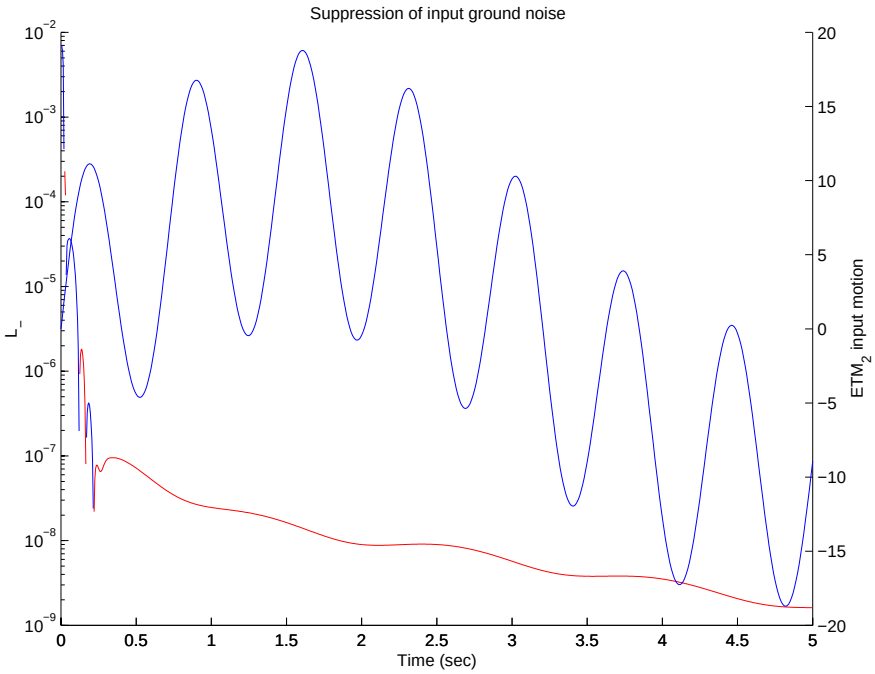

Figure 4: Suppression of input ground noise. The blue sinusoid (right-hand linear scale) is the motion placed on the ETM_2 test mass to simulate L_- ground motion (the other masses had pendulum motion from zero initial displacement); the red and blue lower curve (left-hand log scale) is the resulting closed-loop L_- displacement (red are negative values; blue, positive) showing acquisition and resulting suppression of the noise. Lock was acquired at approximately 0.2 seconds.

The first three items below are of the former category, though I do not believe that they are difficult; simply a matter of design details which have not yet been resolved.

- Switch to detection mode stably (following PNI example).
- Frequency and gain crossovers to the MC length controls, PSL VCO, and IFO actuators. This does not require the same careful design as the detection mode controllers, because noise is not an issue here.
- Physical triggers. The triggers currently used may need to be modified somewhat – 0.4 μW may be an unrealistic level of discrimination to expect from the transmitted light sensors (Table 1). The triggers should also be proportional to determining values, *e.g.*, the PSL power.
- Explore gain/bandwidth/initial conditions phase space systematically.
- Evolution of SMAC as a diagnostic tool for LIGO turn-on; verify against the IFO and other models.
- The effect of alignment on lock acquisition.

Those seeking further edification on lock acquisition may consult [10], where many of these issues have been explored in more detail.

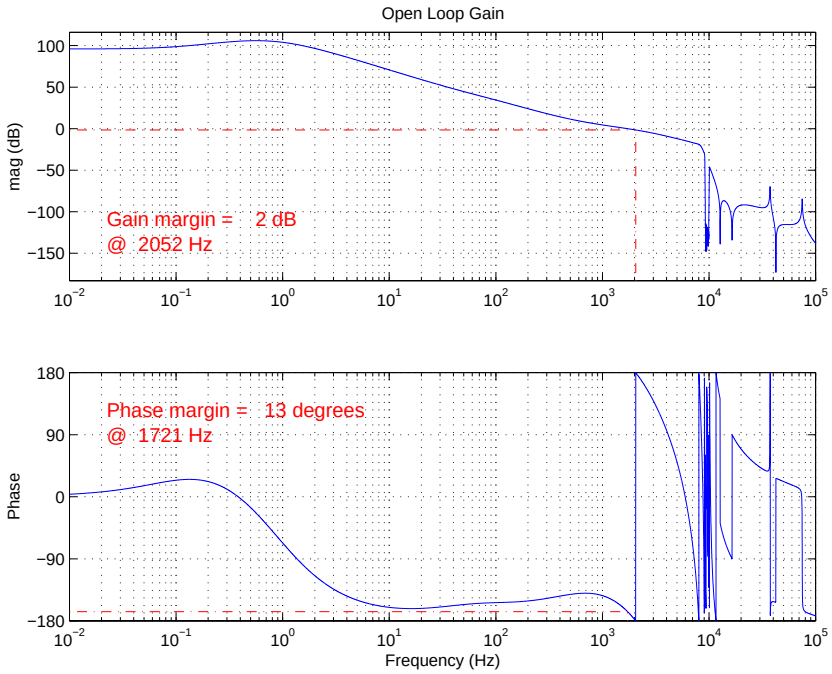

Figure 5: Open loop gain transfer function – IFO differential mode (L_-) from S_{AQ}. The notch has a depth of -123 dB.

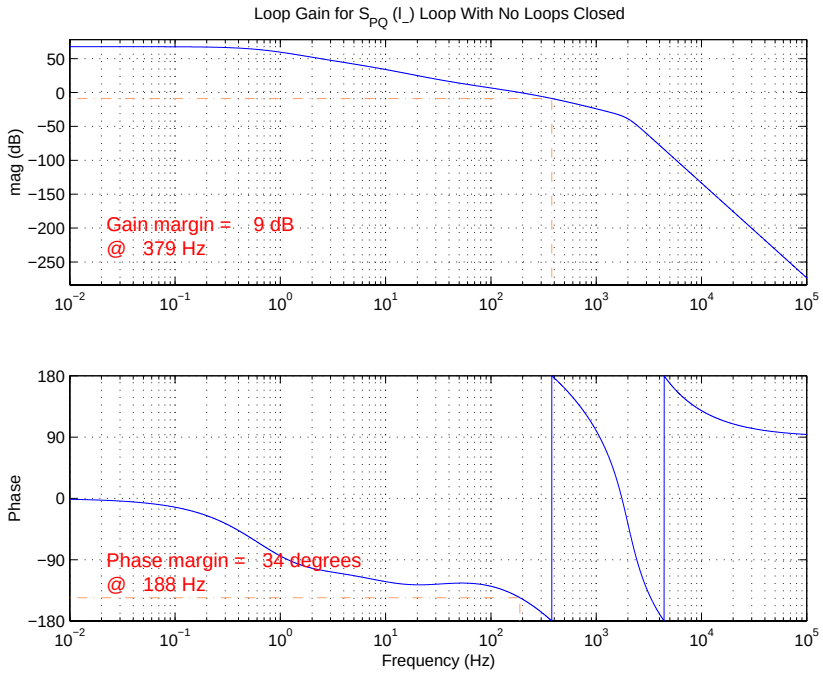

Figure 6: Loop gain transfer function – Michelson differential mode (l_-) from S_{PQ}, State 3

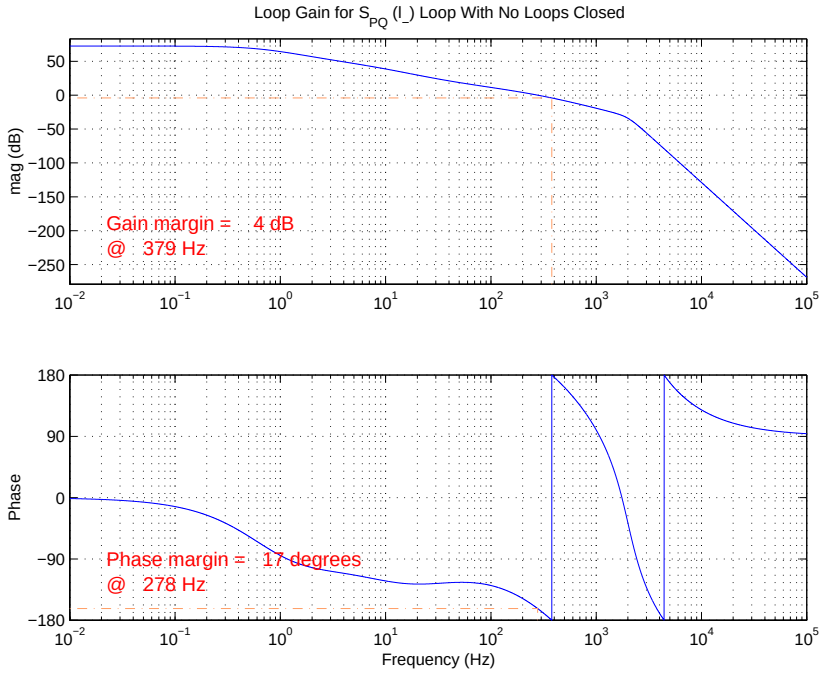

Figure 7: Loop gain transfer function – Michelson differential mode (l_-) from S_{PQ}, State 4

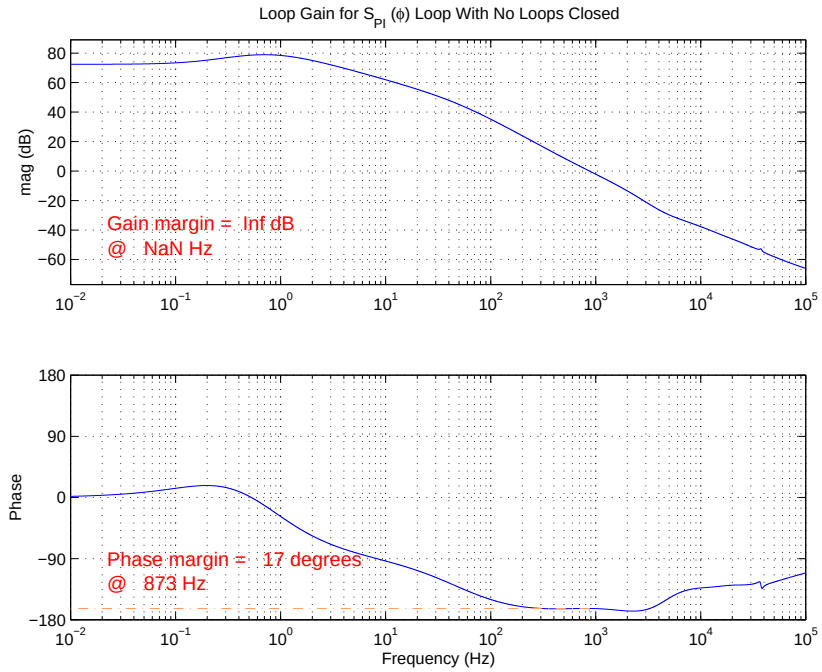

Figure 8: Loop gain transfer function – source phase (ϕ) from S_{PI}, State 3

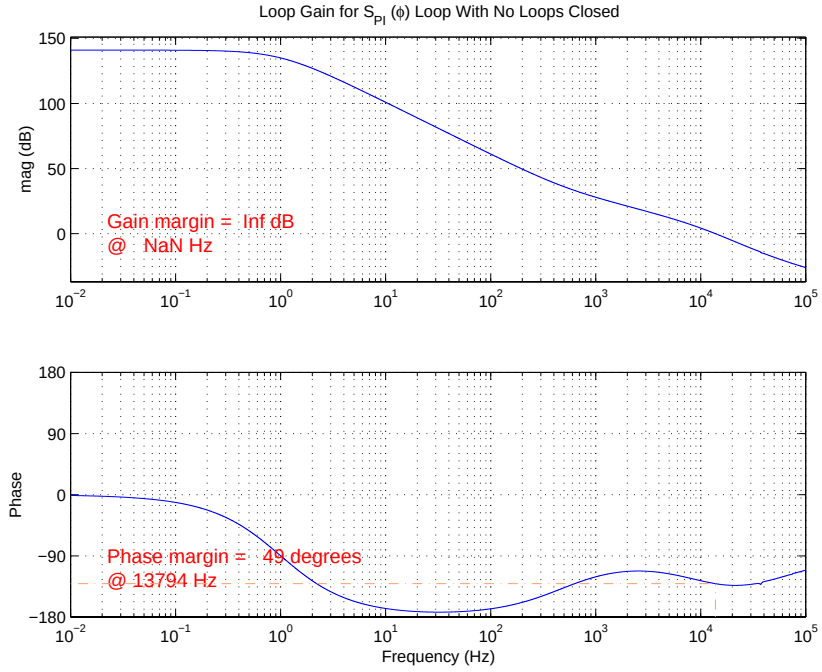

Figure 9: Loop gain transfer function – source phase (ϕ) from S_{PI}, State 4

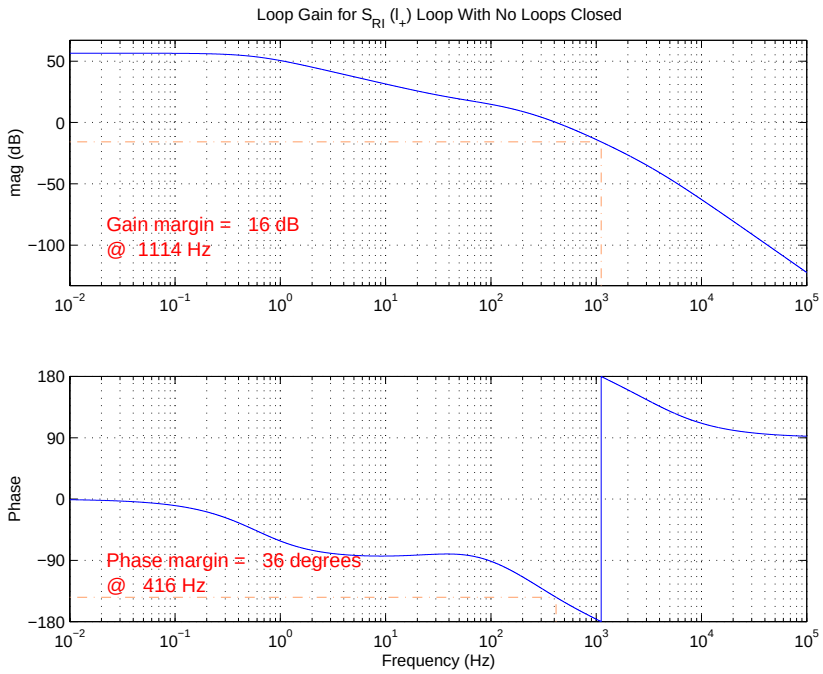

Figure 10: Loop gain transfer function – Michelson common mode (l_+) from S_{RI}, State 3

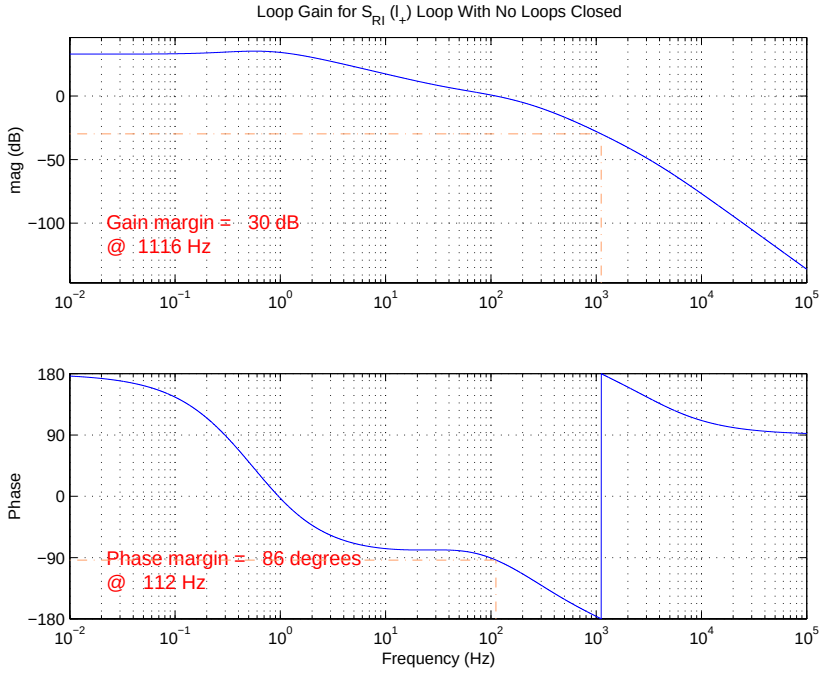

Figure 11: Loop gain transfer function – Michelson common mode (l_+) from S_{RI}, State 4

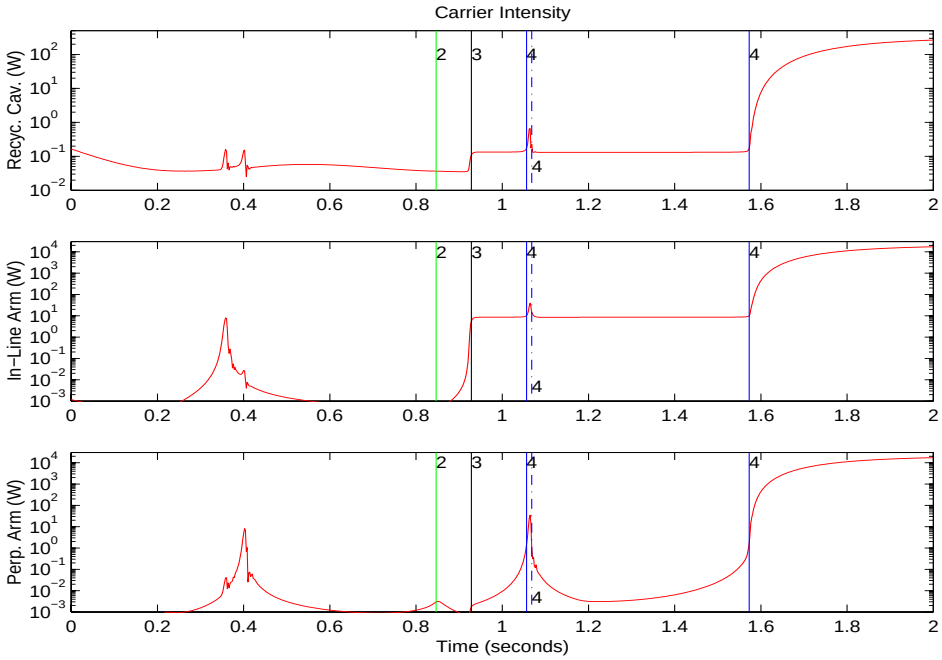

Figure 12: Lock acquisition sequence showing the carrier power in each cavity as it transitions through the acquisition states. The initial conditions for this simulation were chosen to accentuate the transitions between states.

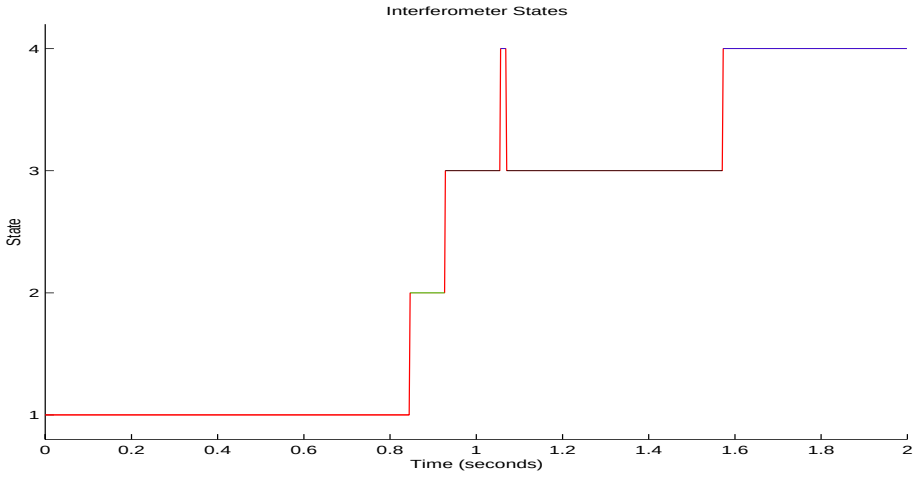

Figure 13: State indicator.

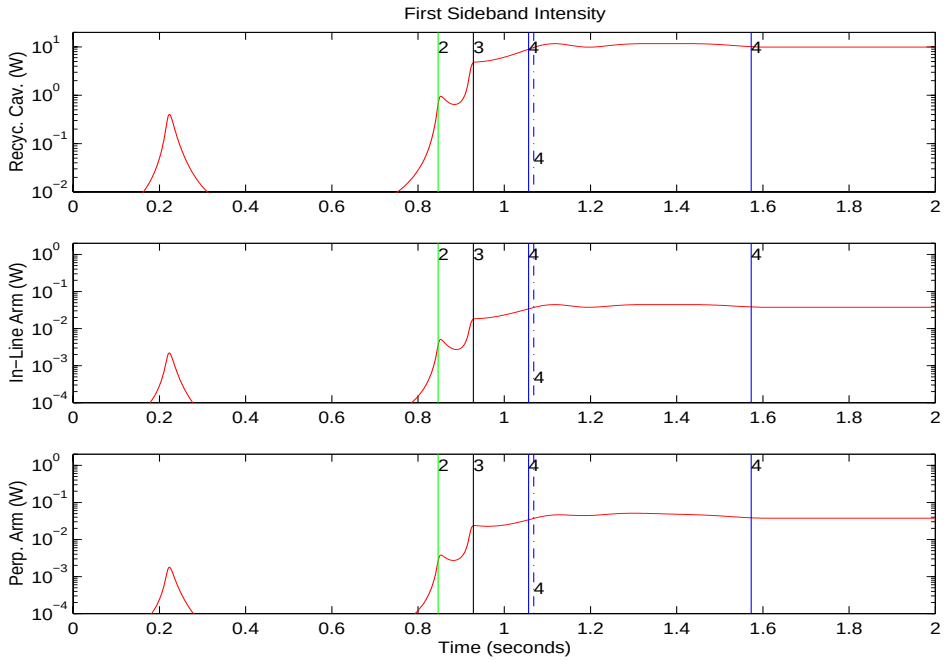

Figure 14: Lock acquisition sequence showing the sideband power in each cavity.

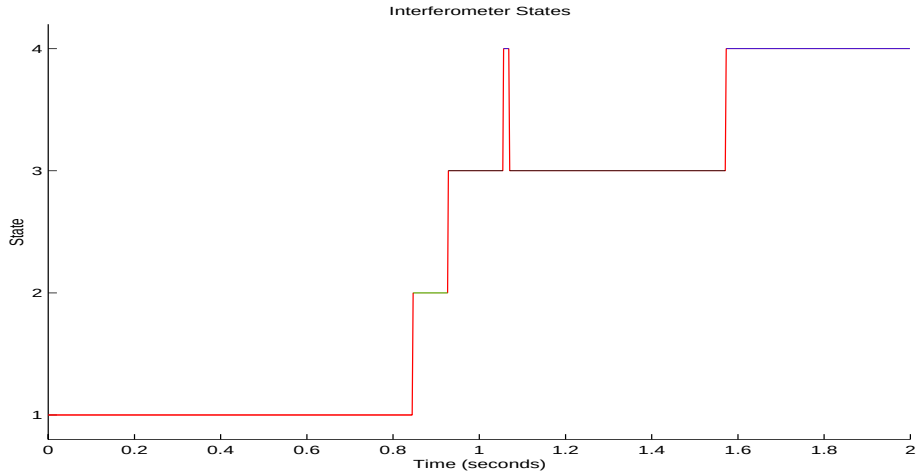

Figure 15: State indicator.

References

[1] Fritschel, P. *et al.*, *Preliminary Design Review*, LIGO-G970192, July 24, 1997, and Fritschel, P., *et al.*, *Length Sensing and Control Subsytem Preliminary Design*, LIGO-T970122, July 18, 1997.

[2] Gabriela Gonzalez's timetraces.m and velhist.m programs (`/home/ware/smac/LSC/MirrorVelocities`).

[3] Needels, L., Redding, D., and Sievers, L., *Single Mode Acquisition Code User Manual*, LIGO-T980018, Jan. 16, 1998.

[4] An, Yang, *et al.*, **Optics Letters**, v.20 No. 9, p. 1068, May 1, 1995.

[5] Personal communication from Jay Heefner, March 26, 1998.

[6] Abbott, R. *Infrared Pre-stabilized Laser Electronics Design Requirements*, LIGO-T970115, pg. 14, Sec. 3.1.1.1.2, Sept. 25, 1997.

[7] Kawamura, S., *et al.*, *Large Optics Suspension Final Design (Mechanical System)*, LIGO-T970158, Sep. 18, 1997.

[8] Regehr, M., *Signal Extraction and Control for an Interferometric Gravitational Wave Detector*, LIGO-P940002, August 1, 1994.

[9] Sigg, D., *et al.*, *Frequency Response of the* LIGO *Interferometer*, LIGO-T970084, Feb. 2, 1997.

[10] Ware, B., *The* BIG BOOK *of* LIGO *Lock Acquisition Design*, LIGO-T980066, ongoing.